Evaluation of Flow-Induced Vibration of Cruciform Control Rod Guide Tubes Using Numerical Flow Analysis

Norimichi Yamashita[1)], Shinichi Kawamura[1)], Tsuyoshi Hagiwara[2)], Noboru Saito[2)], Kumiaki Moriya[3)] and Larry Fennern[4)]

1) Tokyo Electric Power Company, Tokyo, Japan
2) Toshiba Corp,. , Yokohama, Japan
3) Hitachi Ltd., , Hitachi, Japan
4) GE Nuclear Energy, San Jose, CA

ABSTRACT

The control rod guide tube (CRGT) for the next generation ABWR (ABWR-II), being developed by the Japanese BWR Utilities and Plant Suppliers, has a cruciform shape in contrast to the cylindrical one used in conventional BWR reactor design. This design change is due to the use of larger size fuel bundles and K lattice core. The new design may have potential for flow-induced vibration (FIV) because the cruciform CRGT hydraulic resistance against lateral flow is considered to be larger than the conventional one.

Some modifications of analysis methods to evaluate FIV are reported in this paper. The introduction of porous media for the structure modeling is one such modification. Improvement in accuracy was successfully confirmed by comparison between analysis results and measured stresses of the ABWR. In this analysis, an ordinal forcing coefficient for cylindrical structures was used for the CRGT of the current ABWR. Flow-induced vibration stresses on the cruciform CRGT were then estimated by this new method, and its results show that the stress amplitudes are within the level of allowance. Design verification will continue as a 1/5 scale reactor model test in the next phase.

INTRODUCTION

The control rod guide tube (CRGT) for the next generation ABWR (ABWR-II), being developed by the Japanese BWR Utilities and Plant Suppliers, has a cruciform shape in contrast to the cylindrical one used in conventional BWR reactor design. This design change is due to the use of larger size fuel bundles and K lattice core. The new design may have potential for flow-induced vibration because the cruciform CRGT hydraulic resistance against lateral flow is considered to be larger than the conventional one.

It is not easy to evaluate flow-induced vibration (FIV) for the lower plenum of a BWR Reactor Pressure Vessel precisely because of the complexity of its structure. Therefore, actual scale model tests have been required in the past. Recently, the evaluation method using numerical flow analysis was formulated and we set a goal to establish an FIV evaluation method, which may eliminate the need of actual scale model tests in the future, by improvement of numerical flow analysis for the structures in the lower plenum.

In this specific research, we estimate the FIV stresses of cruciform CRGTs by using this method, viz., combining the measurement of fluctuating fluid force in cross and parallel flow for cruciform tubes in a 1/10 scale model test at normal temperature and a three-dimensional numerical analysis of flow inside the ABWR-II reactor. However, for circular components, which are the Control Rod Drive Housings (CRDHs), we use existing data from the conclusive evidence tests of ABWR.

EVALUATION METHOD

During the development of the ABWR, a full scale (1/1 scale) test was done. However, a 1/5 scale test, which simulated the lower plenum, and a numerical flow analysis were also examined to verify the integrity of components in the lower plenum during the ABWR development [1]. Validity of these means to verify integrity was eventually evaluated by comparing the results of the 1/1 scale test and the 1/5 scale test. These results also agreed well with those from measurement in an actual ABWR plant, Kashiwazaki-Kariwa nuclear power station unit 6 of Tokyo Electric Power Company (K-6)[2]. Useful information for the design of cylindrical structures was obtained with improved prospects that an actual scale test might not be necessary considering improvements in numerical flow analysis.

Fig.1 shows the flow chart of the evaluation method using small scale test data and numerical flow analysis and its specific application in this investigation for the cruciform CRGTs of ABWR-II. At first, frequency characteristics of fluctuating fluid force for cruciform cylinders were measured by small scale experiment. They were reduced to non-dimensional power spectrum density (PSD) using representative length (width of test cylinder) and flow velocity. On the other hand, distribution of flow velocity at the ABWR-II lower plenum was analyzed by the numerical method. Power spectrum densities of fluid force on CRGTs/CRDHs in the actual reactor were calculated by substituting these resultant velocities into the reduced PSD. Using these calculated forces on CRGTs/CRDHs, the FIV stress of structures was evaluated by vibration analysis.

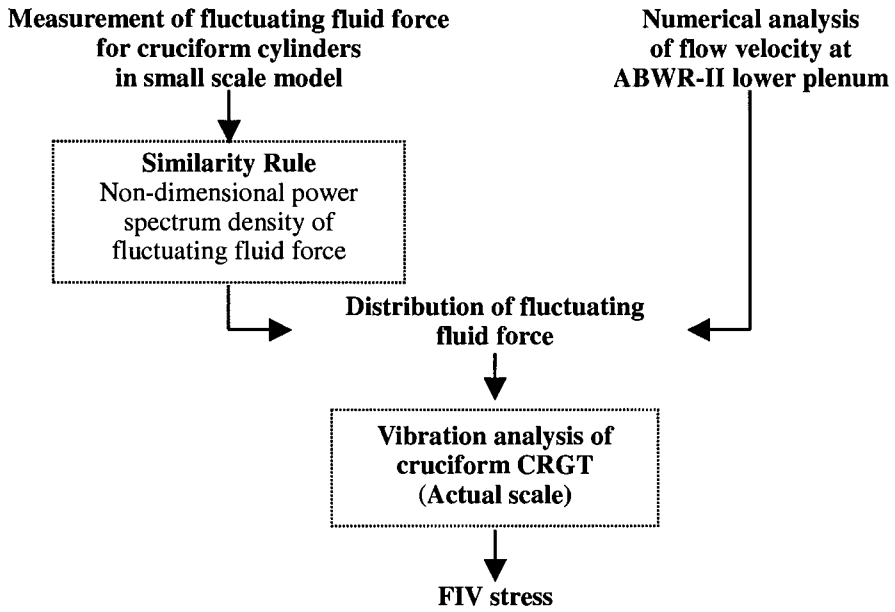

Fig.1 The evaluation method of FIV stress at lower plenum structures

EXPERIMENT

Experimental apparatus

The test section was duct type and made of acrylic resin to measure flow velocity by particle trace velocimetry (PTV). The entire length was about 1700 mm and the distance from an inlet of the duct to the center of installed test cylinders was about 1350 mm (nine times of hydraulic diameter).

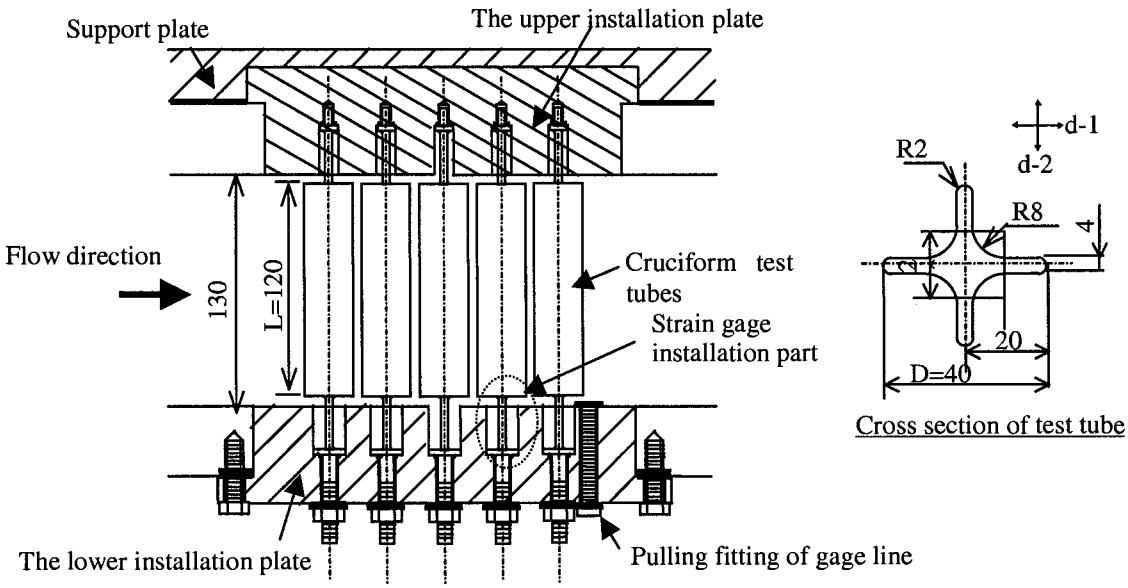

Fig.2 The installation of cruciform test tubes

The cross section form of the test tube was 1/10 scale of an actual cruciform CRGT. The end part of test tube was the measurement part for the strain gauges installation, and strain gauges were installed in 2 directions (d-1 and d-2) of the cross wing directions to measure the fluctuating fluid force. The length of test tube was 3D (D = width of test tube) to the cross flow test, and 6D to the parallel flow test. Fig.2 shows the cruciform test tube installation outline in cross flow. Both ends of test tubes were fixed by up-down caps and installed in the duct.

Test cases

There were three kinds of test cases. The first case (Case-1) was for the tubes located inside in cross flow, the second (Case-2) was for the tubes located front side, and the third (Case-3) was the test for parallel flow. In Case-1, there were two patterns of in-flow angles to the cruciform wing, 0°and 45°,and the inside cylinders were the targets of measurement. As for Case-2, the front array of actual cruciform CRGTs was simulated based on the element of 4×4 test tubes. There were 15 patterns in the total, which made array patterns and in-flow angles as parameters and the tubes located on the front side of the array were the targets. In Case-3, there was only one pattern and an inside tube was the target. Fig.3 shows the representative examples of Case-1 and Case-2.

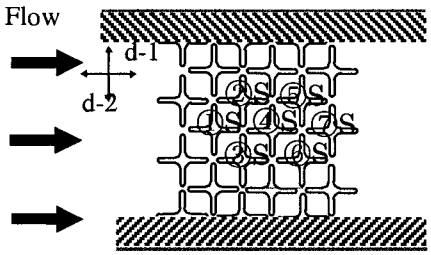

Fig.3 (a) A test array for inside cylinders (Case-1)

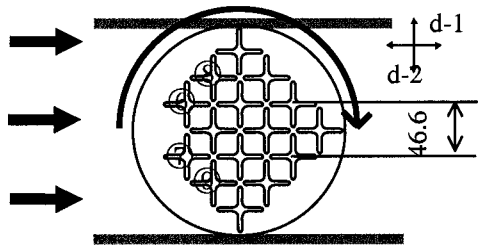

Fig.3 (b) A test array for front cylinders (Case-2)

Experimental condition

The goal for the flow velocity range was from 0 m/s to 3 m/s, and the fluctuating fluid force was measured within this range for several points under the steady state conditions. The representative flow velocity was the gap mean flow velocity for Case-1 and Case-3, and the mean flow velocity near the tip of cruciform wing measured by PTV for Case-2. The temperature was about 20°C and the maximum Reynolds number was about 1.2×10^5.

Experimental results

Fig.4 shows the example of the relation between flow velocity and fluctuating fluid force in Case-2. The relationship of the representative flow velocity U and fluid force F' can be written as Eq.(1) using fluctuating fluid force coefficient C', representative length (width of test cylinder) D and the length of test cylinder L;

$$F'_{r.m.s.} = C' \cdot \frac{1}{2} \rho U^2 \cdot DL \tag{1}$$

where, ρ [kg/m^3] is the fluid density. From Eq.(1), the value of fluid force for different scale structure can be found giving representative length and flow velocity because C' is the non-dimensional coefficient. Therefore, power spectrum density (PSD) of fluid force P_F (f) [N^2/Hz] can be reduced as non-dimensional PSD $\Phi(S)_F$ like Eq.(3) using non-dimensional frequency S written as Eq.(2). The frequency characteristics of fluid force for different scale structures can be found giving $\Phi(S)_F$ representative length and flow velocity as well as fluid force.

Non-dimensional frequency:
$$S = \frac{f \cdot D}{U} \tag{2}$$

NPSD:
$$\Phi(S)_F = \frac{P_F(f)}{\left(\frac{1}{2} \cdot \rho U^2 \cdot D \cdot L\right)^2} \cdot \frac{U}{D} \tag{3}$$

We chose the test cylinders of which PSDs indicated maximum for each test case and reduced to non-dimensional PSDs using Eq.(3). These results are shown from Fig.5 to Fig.7. The curves, which envelop each non-dimensional PSD and fluctuating fluid force coefficients complied with them, are expressed as from Eq.(4) to Eq.(6).

$$S < 0.22:\ \Phi(S)_F = 0.0025 \times S^{-0.31}$$
$$S > 0.22:\ \Phi(S)_F = 0.0012 \times S^{-0.8}$$
$$C' = 0.06 \quad (4)$$

$$S < 0.65:\ \Phi(S)_F = 0.12 \times S^{-0.6}$$
$$S > 0.65:\ \Phi(S)_F = 0.11 \times S^{-0.8}$$
$$C' = 0.28 \quad (5)$$

$$S < 0.13:\ \Phi(S)_F = 0.0007$$
$$S > 0.13:\ \Phi(S)_F = 0.00023 \times S^{-0.54}$$
$$C' = 0.02 \quad (6)$$

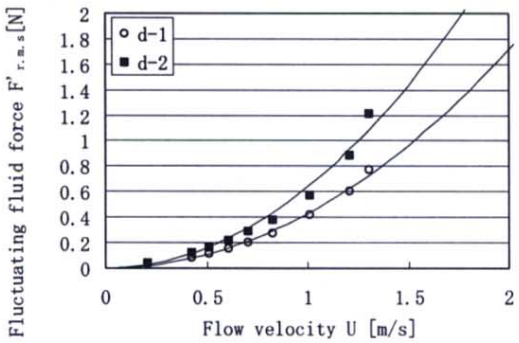

Fig.4 The relation between flow velocity and fluctuating fluid force (Case-2 ex.)

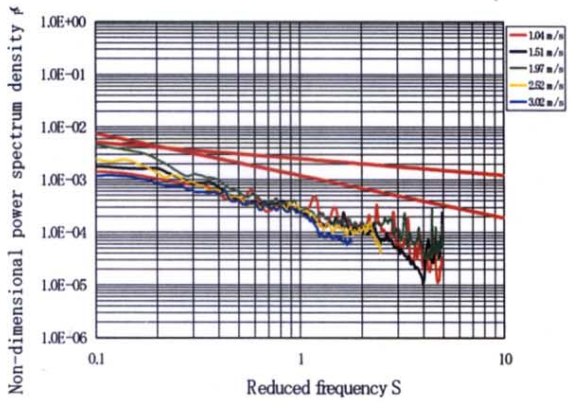

Fig.5 Non-dimensional power spectrum density for inside cylinders (Case-1)

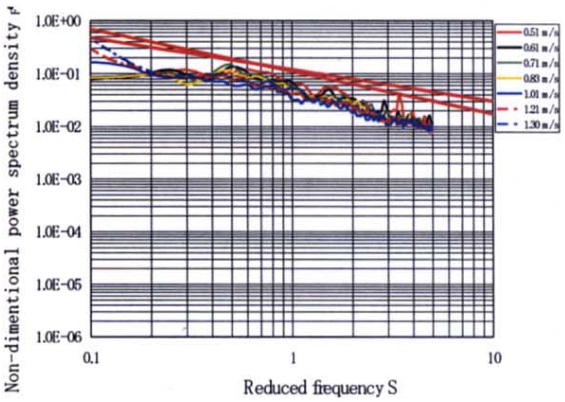

Fig.6 Non-dimensional power spectrum density for front cylinders (Case-2)

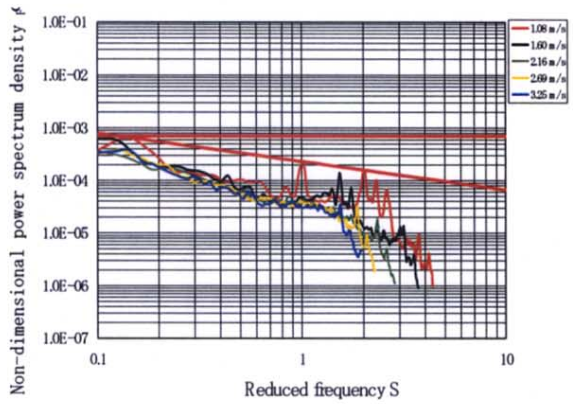

Fig.7 Non-dimensional power spectrum density for parallel flow (Case-3)

NUMERICAL FLOW ANALYSIS

Fig.8 shows the analytical model of ABWR-II lower plenum, which was a 90° sector model. As shown in this figure, the geometry was so complex that it was difficult to be modeled by Cartesian fine mesh only. Therefore, the local porous media method was employed. Usually the surface of an object was represented by a part of the mesh. On the other hand in this method, the surface was located in the cell of the mesh and the fraction of the object in the cell was defined. Using this local fraction, the simulation of the geometry became more detailed without an excessive fine mesh.

The k-ε model was adopted as the turbulent model. The same flow velocity of 10.02 m/s (all pump operation, 111% of core flow rate) was imposed in the spout part of the internal pump as the in-flow boundary condition. For the out-flow boundary condition, the same flow velocity of 4.09 m/s was imposed in the orifices of the core plate to maintain balance with the pump flow rate. Temperature and pressure were the same as the actual condition (temperature; 279°C, pressure; 7.17 Mpa).

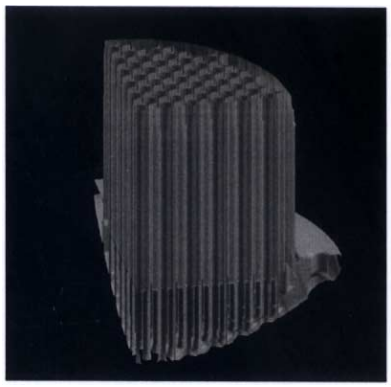

Fig.8 Analytical model of ABWR-II lower plenum

Fig.9 shows the distribution of cross flow velocities in the horizontal section (which is near the upper end of the cruciform CRGTs) and Fig.10 shows the distribution of parallel flow velocity in the vertical section. In the horizontal direction, high flow velocity can be seen at a 45° direction to the wing of the cruciform CRGTs in every two lines, and the state of flow is complex. In the vertical direction, flow velocity near the center of reactor is faster than the circumferential area of the reactor.

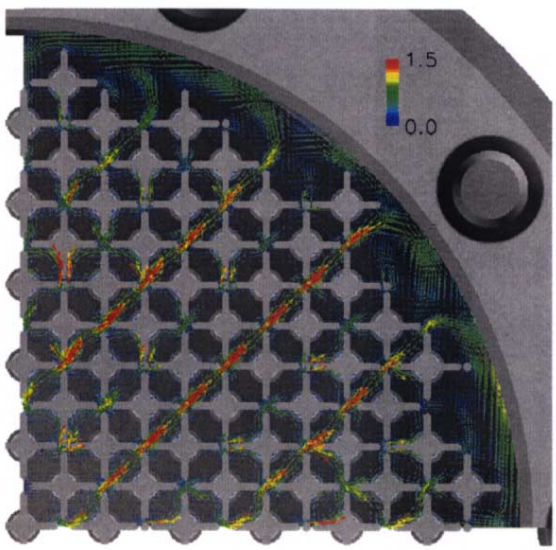

Fig.9 Distribution of velocity at horizontal section near the upper end of cruciform CRGT

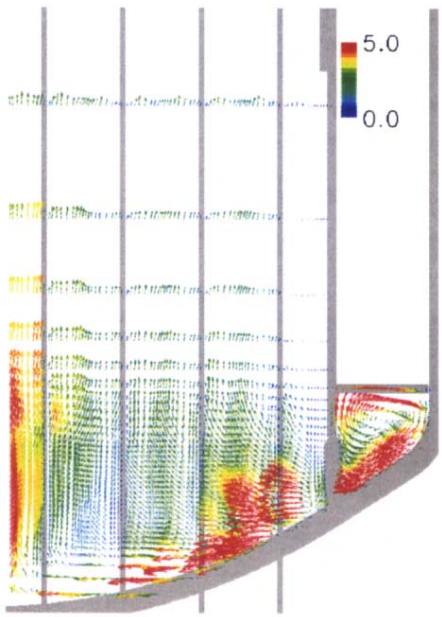

Fig.10 Distribution of velocity at vertical section

EVALUATION OF FIV STRESS

Distribution of fluctuating fluid force was found from the results of the experiments and numerical analysis, and then the stress form FIV were evaluated using vibration analysis. The frequency characteristics of fluid force were found by using the non-dimensional PSD of Eq.(4) for the cruciform CRGTs located inside, Eq.(5) for the CRGTs located in the extreme front row, and Eq.(6) for evaluation of parallel flow. The representative length was the width of the cruciform CRGT (0.3977 m) and the velocity was the mean flow velocity near the tip of cruciform wing in each position of the height. The range of frequency was up to 200 Hz, the natural frequency that the third mode existed in. As for vibration analysis, FIV of these structures was considered as the forced vibration by a random fluctuating force, but the stress was evaluated conservatively as each component of frequency was same phase. Regarding the support condition of structures, the upper end of CRGT was a pinned joint, the joint part of CRGT and CRDH was hinged joint, and the bottom end of the CRDH was rigid joint as Fig.11. The damping coefficient of structures was 1%, crest-factor was 3 and stress concentrate factor was 4.

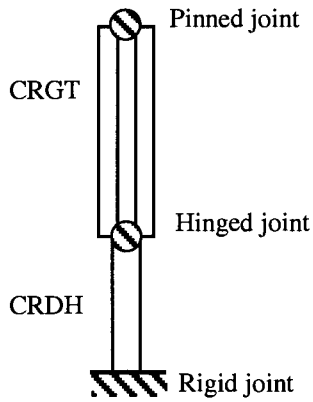

Fig.11 The support condition

Table 1 shows the results of the FIV stress evaluation and Fig.12 shows the comparison of FIV stress. These were stress values at the root part of CRDHs, where the stress reached a maximum value, and are reported as the square root of the sum of FIV stress of the cross flow squared and parallel flow squared.

It can be observed that the part where the fastest flow velocity occurs is near the spout parts of the internal pump by numerical flow analysis. Though the position of No.(e) isn't the highest point of flow velocity, No.(e) indicates the maximum stress value (19.8 N/mm^2) among CRGTs located in the extreme front row. It is considered that the stress occurring in the structures is influenced not only by flow velocity of the CRDHs parts, but also by the cruciform CRGTs parts largely, and the flow velocity near the CRGT part of No.(e) indicates high value.

No.(q) which is located inside indicates the maximum value of 63.5 N/mm^2 among all tubes. Though the fluctuating fluid force coefficient for the inside cruciform tubes in the cross flow is about 1/5 times that for the front side, the stress of the tube which located in the center of the reactor indicates the maximum value. It is reasoned to be maximum because the bending moment of the center cylinder, which has longest CRDH (about 1.4 m), and the velocity of parallel flow are larger than for the other tubes. However, this maximum stress value is less than the fatigue limit of austenitic stainless steel (85 N/mm^2).

CONCLUSIONS

It was estimated that the maximum stress which occurs in the cruciform CRGTs/CRDHs of ABWR-II from FIV was about 19.8 N/mm^2 for the tubes located in the front row and about 63.5 N/mm^2 for the tubes located in the inside row. However, the maximum value was less than the fatigue limit of austenitic stainless steel.

While we have a goal to substitute this evaluation for actual scale tests in the future, it was observed that the state of flow was very complex at reactor lower plenum of ABWR-II. To research this influence and to find more realistic FIV stress, we will continue investigation of the distribution of FIV stress by the 1/5 scale reactor model test in the next phase.

Table1. The result of FIV stress analysis

	Number	Stress [N/mm^2]*	f_n [Hz]
Front cylinders	(a)	3.3	31.6
	(b)	8.8	29.3
	(c)	7.8	30.9
	(d)	15.5	29.6
	(e)	19.8	28.8
	(f)	12.1	32.3
	(g)	18.2	28.8
	(h)	9.1	29.6
	(i)	6.4	30.9
	(j)	9.2	29.3
	(k)	4.3	31.6
Inside cylinders	(l)	3.9	28.8
	(m)	6.2	27.4
	(n)	9.5	28.5
	(o)	7.3	27.4
	(p)	3.9	28.8
	(q)	63.5	17.1
	(r)	19.4	20.2

*Peak value

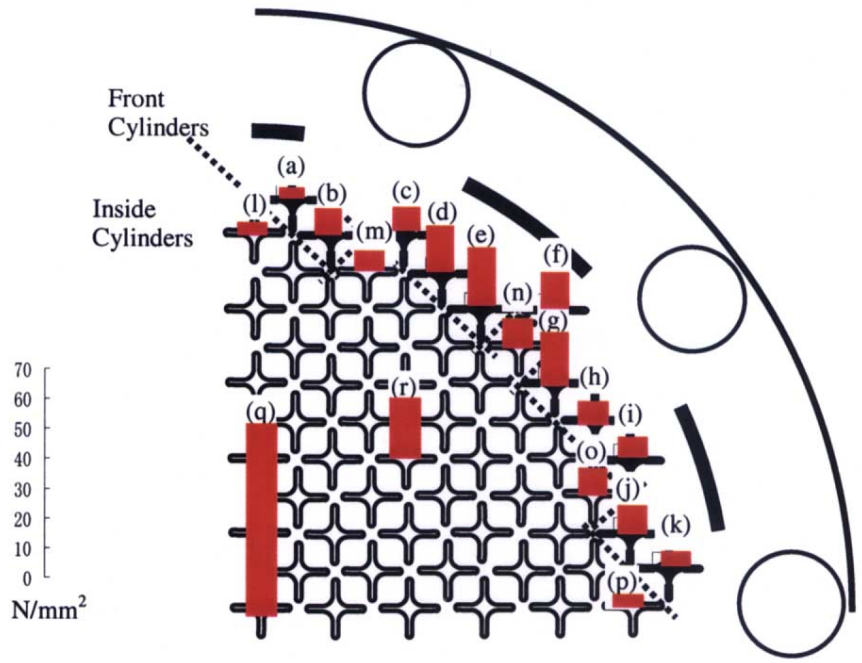

Fig.12 Comparison of FIV stress

REFERENCES

1. N.Satio, T.Hgiwara and H.Miyano, "Flow-Induced Characteristics of ABWR Reactor Internal Components," *ASME PVP-Vol.363, Flow-Induced Vibration and Transient Thermal-Hydraulics*, 1998, pp.65-71
2. K.Hasegawa and others, "FLOW INDUCED VIBRATION TESTING OF ABWR REACTOR PRESSURE VESSEL INTERNAL COMPONENTS," *ASME/JSME/SFEN 6th ICONE, Track3 Structural Integrity, Dynamic behavior and seismic Design*, ICONE-620, 1998.